Structural and vibrational properties of $K_3Fe(MoO_4)_2(Mo_2O_7)$—a novel layered molybdate

2009 J. Phys.: Condens. Matter 21 095402

(http://iopscience.iop.org/0953-8984/21/9/095402)

J. Phys.: Condens. Matter **21** (2009) 095402 (8pp) doi:10.1088/0953-8984/21/9/095402

Structural and vibrational properties of $K_3Fe(MoO_4)_2(Mo_2O_7)$—a novel layered molybdate

M Mączka[1,5], A Pietraszko[1], W Paraguassu[2], A G Souza Filho[3], P T C Freire[3], J Mendes Filho[3] and J Hanuza[4]

[1] Institute of Low Temperature and Structure Research, Polish Academy of Sciences, PO Box 1410, 50-950 Wrocław 2, Poland
[2] Departamento de Fisica, Universidade Federal do Maranhão, São Luis-MA, Brazil
[3] Departamento de Fisica, Universidade Federal do Ceara, Fortaleza, Ceara, Brazil
[4] Department of Bioorganic Chemistry, Faculty of Industry and Economics, University of Economics, ulica Komandorska 118/120, 53-345 Wrocław, Poland

E-mail: m.maczka@int.pan.wroc.pl

Received 12 December 2008
Published 29 January 2009
Online at stacks.iop.org/JPhysCM/21/095402

Abstract

The new compound $K_3Fe(MoO_4)_2(Mo_2O_7)$ was synthesized and characterized by a single-crystal x-ray structure determination, and IR and Raman spectroscopic studies. The crystal structure at room temperature and ambient pressure is monoclinic, space group $C2/c$, with the unit cell dimensions $a = 32.885(7)$, $b = 5.7220(11)$, $c = 15.852(3)$ Å, $\beta = 91.11°$, $Z = 8$. The FeO_6 octahedra are joined by corners with MoO_4^{2-} tetrahedra and $Mo_2O_7^{2-}$ units. Some of the K^+ ions form layers in the $b \times c$-plane. The origin of various Raman and IR vibrational modes is discussed. These results indicate that a clear energy gap exists between the stretching and remaining modes. High-pressure Raman scattering studies were also performed. These studies showed the onset of two reversible first-order phase transitions near 1.2 and 7.4 GPa, which are associated with strong distortion of the MoO_4^{2-} and $Mo_2O_7^{2-}$ units.

1. Introduction

Iron molybdates attract considerable attention because they exhibit interesting structural, catalytic, ferroelastic and magnetic properties [1–9]. For instance, $KFe(MoO_4)_2$ and $RbFe(MoO_4)_2$ molybdates have gained considerable attention, since these compounds constitute rare examples of nearly two-dimensional 'triangular' antiferromagnets available in single-crystal form [8, 9]. $KFe(MoO_4)_2$ also exhibits interesting ferroelastic phase transitions [6] and $NaFe_4(MoO_4)_5$ may find application as a solid state electrolyte with sodium cation conductivity [10].

The chemical coordination of the molybdenum atoms in alkali metal iron molybdates is usually tetrahedral. The only exception is $Na_3Fe_2Mo_5O_{16}$, in which three MoO_6 octahedra are connected by edge-sharing, forming Mo_3O_{13} clusters [3]. $Mo_2O_7^{2-}$ units were not found in any iron molybdate, and only a few molybdate structures containing both MoO_4^{2-} tetrahedra and $Mo_2O_7^{2-}$ dimers are known. Actually, these units were found for instance in $Ln_2Mo_4O_{15}$ (Ln = Y, Dy, Ho, Tm), which exhibit anomalous thermal expansion behavior [11], and $Eu_6Mo_{10}O_{39}$ [12].

In this paper, we report x-ray diffraction, Raman and infrared (IR) studies of a novel layered iron molybdate, $K_3Fe(MoO_4)_2(Mo_2O_7)$. High-pressure Raman scattering studies on this material were also performed. The aim of these studies is to gain information on the ambient pressure structure and vibrational properties of this molybdate as well as structural changes occurring in the $K_3Fe(MoO_4)_2(Mo_2O_7)$ crystal under hydrostatic pressure and the pressure dependence of the phonon properties. The present studies revealed that this novel molybdate exhibits two reversible first-order phase transitions at about 1.2 and 7.4 GPa, which are associated with strong distortion of the MoO_4^{2-} and $Mo_2O_7^{2-}$ units.

[5] Author to whom any correspondence should be addressed.

Table 1. Crystal data and structure refinement for $K_3Fe(MoO_4)_2(Mo_2O_7)$.

Empirical formula	$FeK_3Mo_4O_{15}$
Formula weight	796.91
Temperature (K)	293(2)
Wavelength (Å)	0.71073
Crystal system, space group	Monoclinic, $C2/c$
Unit cell dimensions (Å)	
a	32.885(7)
b	5.7220(11)
c	15.852(3)
β (deg)	91.11
Volume (Å^3)	2982.3(10)
Z, calculated density (Mg m^{-3})	8, 3.550
Absorption coefficient (mm^{-1})	5.131
$F(000)$	2968
Crystal size (mm)	$0.19 \times 0.17 \times 0.15$
Θ range for data collection (deg.)	3.54–46.29
Limiting indices	$-64 \leqslant h \leqslant 61$, $-8 \leqslant k \leqslant 9$, $-20 \leqslant l \leqslant 32$
Reflections collected/unique	26 341/10 254 ($R_{int} = 0.0817$)
Completeness to $\Theta = 46.29$	77.9%
Absorption correction	None
Refinement method	Full-matrix least-squares on F^2
Data/restraints/parameters	10 254/0/209
Goodness-of-fit on F^2	1.054
Final R indices [$I > 2\sigma(I)$]	$R_1 = 0.0428$, $wR_2 = 0.0730$
R indices (all data)	$R_1 = 0.0704$, $wR_2 = 0.0775$
Extinction coefficient	0.000 43(2)
Largest diff. peak and hole (e Å^{-3})	2.565 and −3.125

2. Experimental details

Single crystals of $K_3Fe(MoO_4)_2(Mo_2O_7)$ were grown by cooling of the mixture containing K_2CO_3, Fe_2O_3 and MoO_3 in the ratio 2:1:6. The mixture was placed in a platinum crucible, heated to 800 °C, kept at this temperature for 40 h, cooled at a rate of 2–500 °C and then cooled at a rate of 5 °C to room temperature. The obtained light green crystals of optical quality were extracted from the crucible by washing with hot water.

The crystal sample of dimensions given in table 1 was selected for x-ray diffraction data collection with a four-circle diffractometer KM-4/CCD (Oxford diffraction) at room temperature. Graphite monochromated Mo Kα radiation (λ = 0.071073 nm) was generated at 50 kV and 23 mA. A single image for 1.2° rotation around the ω axis was obtained in 40 s and the full set of x-ray diffraction in the 2θ angle was collected over the range from 3° to 93°. The intensities of the reflections were recorded in 800 frames. Analytical absorption correction for all samples was calculated with the CrysAlis procedure [13]. Details of data collection and structure refinement are presented in table 1. The crystal structure was solved using the direct method—the SHELXL-97 program [14]. The same program was used for the successive refinement cycles of the crystal structure.

IR studies were performed with a Biorad 575C FT-IR spectrometer. Polycrystalline spectra were measured as KBr pellets in the 1300–400 cm^{-1} region and in Nujol suspension for the 500–40 cm^{-1} region. The Raman spectra were obtained with a triple-grating spectrometer Jobin Yvon T64000, which is equipped with a N_2-cooled charge coupled device detection system. The 514.5 nm line of an argon laser was used as excitation. An Olympus microscope lens with a focal distance of 20.5 mm and a numerical aperture of 0.35 was used to focus the laser beam on the sample surface. The high-pressure experiments were performed using a diamond anvil cell with a 4:1 methanol:ethanol mixture as the transmission fluid. The spectrometer slits were set for a resolution of 2 cm^{-1}.

3. Results and discussion

3.1. Structure determination

The room temperature and ambient pressure phase of $K_3Fe(MoO_4)_2(Mo_2O_7)$ was determined as being monoclinic with space group $C2/c$ (C^6_{2h}, No. 15). It comprises eight chemical formula units per unit cell with the lattice parameters a = 32.885(7), b = 5.7220(11), c = 15.852(3) Å and monoclinic angle $\beta = 91.11°$. The crystal data, experimental details and the structure refinement parameters are listed in table 1.

The structural motif consists of the iron–oxygen octahedron, two symmetrically distinct MoO_4^{2-} tetrahedra, the $Mo_2O_7^{2-}$ dimer and three symmetrically distinct K^+ ions (see figure 1). The atomic position parameters are listed in table 2 and the selected bond lengths and angles are presented in table 3. The octahedron of FeO_6 indicates significant distortion (the O–Fe–O angles change from 88.02(7)° to 92.08(8)°). The Mo–O distances are situated in the range from 1.721(2) to 1.8064(15) Å and 1.7140(16) to 1.7958(14) Å for the tetrahedron Mo(1) and Mo(2), respectively. This result indicates that both MoO_4^{2-} tetrahedra have similar distortion. In the $Mo_2O_7^{2-}$ group, the bonds between the molybdenum atoms and the bridging oxygen atom are much

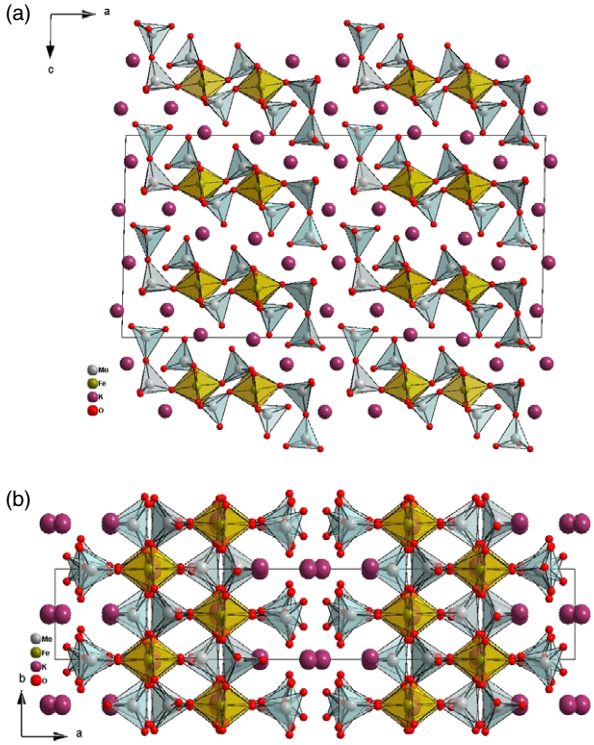

Figure 1. (a) View of the crystal structure of $K_3Fe(MoO_4)_2(Mo_2O_7)$ along the *b*-axis and (b) along the *c*-axis.

(This figure is in colour only in the electronic version)

Table 2. Fractional atomic coordinates ($\times 10^4$) and equivalent isotropic displacement parameters (Å $\times 10^3$) for $K_3Fe(MoO_4)_2(Mo_2O_7)$. *U* (eq) is defined as one-third of the trace of the orthogonalized U_{ij} tensor.

	x	*y*	*z*	*U* (eq)
Mo(1)	1498(1)	4 853(1)	1189(1)	13(1)
Mo(2)	2185(1)	−4 875(1)	3422(1)	11(1)
Mo(3)	686(1)	−37(1)	2319(1)	13(1)
Mo(4)	569(1)	9 621(1)	−20(1)	17(1)
Fe(1)	1805(1)	−12(1)	2406(1)	11(1)
K(1)	131(1)	−5 152(1)	1308(1)	22(1)
K(2)	1871(1)	9 685(1)	−123(1)	23(1)
K(3)	1063(1)	−4 777(1)	3654(1)	27(1)
O(34)	1208(1)	−190(2)	2609(1)	21(1)
O(21)	2591(1)	−4 796(2)	2716(1)	19(1)
O(22)	1905(1)	−2 182(2)	3400(1)	16(1)
O(31)	467(1)	2 317(3)	2808(1)	22(1)
O(12)	1495(1)	5 266(3)	108(1)	27(1)
O(23)	1839(1)	−7 227(2)	3195(1)	19(1)
O(33)	453(1)	−2 500(3)	2694(1)	23(1)
O(32)	581(1)	202(3)	1165(1)	27(1)
O(14)	1721(1)	2 035(2)	1420(1)	22(1)
O(11)	1786(1)	7 180(3)	1668(1)	25(1)
O(42)	492(1)	6 694(3)	−251(1)	27(1)
O(13)	1010(1)	4 938(3)	1560(1)	38(1)
O(24)	2376(1)	−5 264(3)	4426(1)	28(1)
O(43)	1037(1)	10 355(3)	−390(1)	40(1)
O(41)	221(1)	11 391(3)	−541(1)	37(1)

longer (1.8608(16) and 1.9069(16) Å) than the remaining Mo–O bonds in this unit (1.707(2)–1.7719(19) Å). Very similar bond lengths in the $Mo_2O_7^{2-}$ unit were found for

Table 3. Selected bond lengths (Å) and angles (deg.).

Mo(1)–O(13)	1.721(2)	K(2)–O(24)#14	2.694(2)
Mo(1)–O(12)	1.7292(16)	K(2)–O(22)#9	2.7462(15)
Mo(1)–O(11)	1.7935(16)	K(2)–O(43)	2.794(2)
Mo(1)–O(14)	1.8064(15)	K(2)–O(12)	2.8410(17)
Mo(2)–O(24)	1.7140(16)	K(2)–O(14)#5	2.8424(16)
Mo(2)–O(21)	1.7599(18)	K(2)–O(23)#6	3.0149(16)
Mo(2)–O(23)	1.7936(15)	K(2)–O(24)#6	3.1163(18)
Mo(2)–O(22)	1.7958(14)	K(2)–O(11)	3.1978(18)
Mo(3)–O(33)	1.7150(16)	K(3)–O(12)#2	2.6987(19)
Mo(3)–O(31)	1.7183(15)	K(3)–O(42)#2	2.8066(19)
Mo(3)–O(34)	1.7719(19)	K(3)–O(33)	2.8140(19)
Mo(3)–O(32)	1.8608(16)	K(3)–O(31)#1	2.8819(18)
Mo(4)–O(43)	1.707(2)	K(3)–O(43)#3	2.952(2)
Mo(4)–O(41)	1.7270(18)	K(3)–O(23)	3.0135(18)
Mo(4)–O(42)	1.7324(15)	K(3)–O(34)	3.1449(17)
Mo(4)–O(32)#5	1.9069(16)	K(3)–O(22)	3.1730(18)
Fe(1)–O(14)	1.9685(15)	K(3)–O(13)#1	3.325(2)
Fe(1)–O(11)#1	1.9880(15)		
Fe(1)–O(34)	1.9972(19)	O(11)–Fe(1)–O(21)	90.71(7)
Fe(1)–O(21)#10	2.0041(18)	O(11)–Fe(1)–O(22)	88.02(7)
Fe(1)–O(23)#5	2.0264(14)	O(11)–Fe(1)–O(14)	90.61(7)
Fe(1)–O(22)	2.0278(14)	O(11)–Fe(1)–O(34)	91.93(7)
K(1)–O(41)#11	2.7190(18)	O(21)–Fe(1)–O(22)	88.16(7)
K(1)–O(42)#8	2.764(2)	O(21)–Fe(1)–O(23)	88.19(7)
K(1)–O(31)#12	2.8350(18)	O(21)–Fe(1)–O(14)	90.52(7)
K(1)–O(33)	2.8582(17)	O(22)–Fe(1)–O(23)	89.77(7)
K(1)–O(13)#1	2.912(3)	O(22)–Fe(1)–O(34)	89.31(7)
K(1)–O(33)#13	2.9347(18)	O(23)–Fe(1)–O(14)	91.57(7)
K(1)–O(42)#1	2.9554(18)	O(23)–Fe(1)–O(34)	89.07(7)
K(1)–O(31)#1	2.9793(18)	O(14)–Fe(1)–O(34)	92.08(8)
K(1)–O(32)#1	3.0526(18)		
K(1)–O(32)	3.4108(18)		

Symmetry transformations used to generate equivalent atoms:
#1 $x, y-1, z$; #2 $x, -y, z+1/2$; #3 $x, -y+1, z+1/2$;
#4 $-x+1/2, y-3/2, -z+1/2$; #5 $x, y+1, z$;
#6 $x, -y, z-1/2$; #7 $x, y+2, z$; #8 $-x, -y, -z$;
#9 $x, -y+1, z-1/2$; #10 $-x+1/2, y+1/2, -z+1/2$;
#11 $-x, -y+1, -z$; #12 $-x, y-1, -z+1/2$;
#13 $-x, y, -z+1/2$; #14 $-x+1/2, y+3/2, -z+1/2$;
#15 $-x+1/2, y-1/2, -z+1/2$; #16 $-x, y+1, -z+1/2$.

$Eu_3Mo_{10}O_{39}$ molybdate [12]. The Mo–O–Mo bridge has a bend configuration and the respective angle is 162.72(11)°.

In the $K_3Fe(MoO_4)_2(Mo_2O_7)$ structure the MoO_4^{2-} and $Mo_2O_7^{2-}$ units are linked through the FeO_6 octahedra into the ribbons running along the crystal *b*-axis and parallel to the $(\bar{1}02)$ plane (figure 1(b)). The FeO_6 octahedra are well separated in the ribbons, and therefore this material may be a suitable model for magnetic interactions. These ribbons are separated by K^+ ions. The presence of layers composed of K^+ ions in the crystal *bc*-plane explains the pronounced cleavage of this crystal.

3.2. Ambient pressure Raman and IR spectra

For the $C2/c$ structure of $K_3Fe(MoO_4)_2(Mo_2O_7)$, group theory predicts $69A_g + 69B_g + 69A_u + 69B_u$ Brillouin zone center modes. From these modes, one A_u and two B_u modes belong to the acoustic branches and, consequently, the optical modes are distributed as $69A_g+69B_g+68A_u+67B_u$. Since the primitive cell comprises two MoO_4^{2-}, one $Mo_2O_7^{2-}$, one Fe^{3+} and three K^+ ions, these ions give rise to $6A_g + 6B_g + 6A_u +$

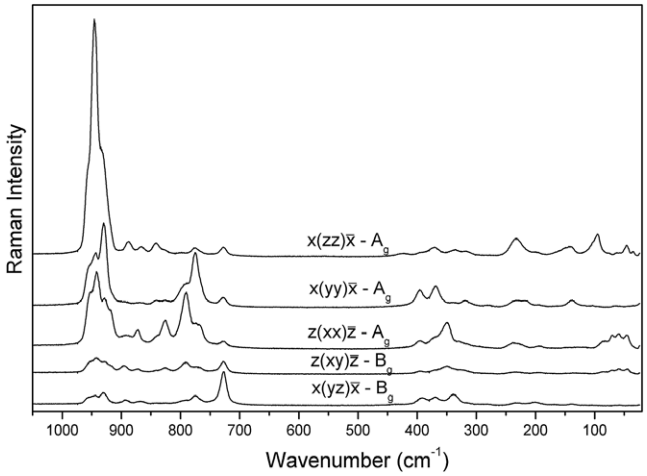

Figure 2. Polarized Raman spectra of $K_3Fe(MoO_4)_2(Mo_2O_7)$.

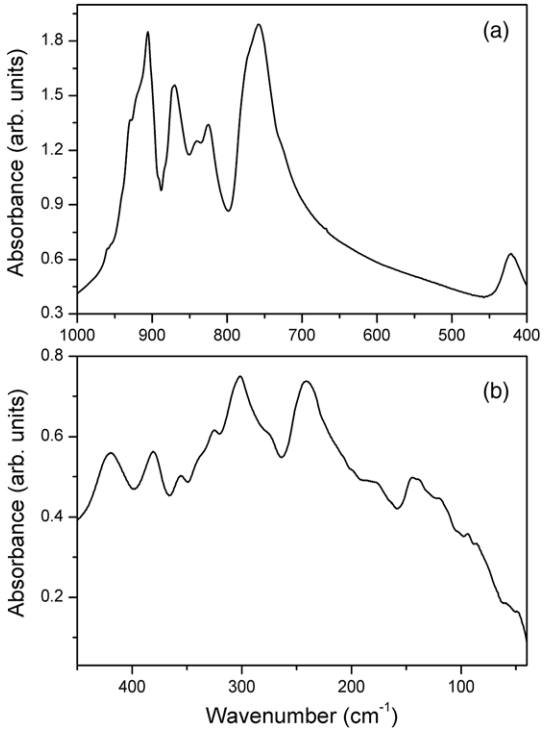

Figure 3. IR spectra in the mid-IR (a) and far-IR (b) region.

$6B_u$, $3A_g + 3B_g + 3A_u + 3B_u$, $3A_g + 3B_g + 3A_u + 3B_u$ and $9A_g + 9B_g + 9A_u + 9B_u$ translational modes, respectively. The number of librational modes is $3A_g + 3B_g + 3A_u + 3B_u$ and $6A_g + 6B_g + 6A_u + 6B_u$ for $Mo_2O_7^{2-}$ and MoO_4^{2-}, respectively. The $18A_g + 18B_g + 18A_u + 18B_u$ internal modes of the MoO_4^{2-} ions can be subdivided into $6A_g + 6B_g + 6A_u + 6B_u$ asymmetric stretching (ν_3), $2A_g + 2B_g + 2A_u + 2B_u$ symmetric stretching (ν_1), $6A_g + 6B_g + 6A_u + 6B_u$ asymmetric bending (ν_4) and $4A_g + 4B_g + 4A_u + 4B_u$ symmetric bending (ν_2) modes. The number of internal modes of the $Mo_2O_7^{2-}$ ions is $21A_g + 21B_g + 21A_u + 21B_u$. By analogy with $P_2O_7^{4-}$ ions, the internal modes can be subdivided into MoO_3 and Mo–O–Mo vibrations. Cornilsen *et al* showed that for a free $P_2O_7^{4-}$ ion with a bent P–O–P bridge the highest symmetry is C_{2v} [15, 16]. Thus the 21 internal modes can be subdivided into the symmetric and asymmetric stretching modes of the PO_3 groups (ν_sPO_3 $(A_1 + B_1)$ and $\nu_{as}PO_3$ $(A_1 + B_1 + B_2 + A_2)$, respectively), symmetric and asymmetric stretching modes of the P–O–P bridge (ν_sPOP (A_1) and $\nu_{as}POP$ (B_1), respectively), bending mode of the P–O–P bridge (δPOP (A_1)), rocking modes of the PO_3 groups (τ $(A_2 + B_2)$) and O–P–O bending modes (δOPO $(3A_1 + 2A_2 + 3B_1 + 2B_2)$) [15–17]. By analogy with $P_2O_7^{4-}$ ions, we can subdivide the internal modes of the $Mo_2O_7^{2-}$ ions of C_1 symmetry into ν_sMoO_3 $(2A_g + 2B_g + 2A_u + 2B_u)$, $\nu_{as}MoO_3$ $(4A_g + 4B_g + 4A_u + 4B_u)$, ν_sMoOMo $(A_g + B_g + A_u + B_u)$, $\nu_{as}MoOMo$ $(A_g + B_g + A_u + B_u)$, $\delta MoOMo$ $(A_g + B_g + A_u + B_u)$, τ $(2A_g + 2B_g + 2A_u + 2B_u)$, and $\delta OMoO$ $(10A_g + 10B_g + 10A_u + 10B_u)$. The A_g and B_g modes are Raman active, and the A_u and B_u modes are IR active.

Room-temperature Raman spectra of the $K_3Fe(MoO_4)_2(Mo_2O_7)$ single crystal, measured in different polarization configurations, as well as the polycrystalline IR spectra, are shown in figures 2 and 3. The observed wavenumbers are listed in table 4. These figures and table 4 show that the modes are observed in two well separated regions, i.e. 960–728 and 423–36 cm^{-1}. The modes in the 960–728 cm^{-1} region can be unambiguously attributed to stretching vibrations of the Mo–O bonds. Our former studies of double molybdates showed that for crystals composed of isolated MoO_4^{2-} tetrahedra the ν_1 modes are observed at higher wavenumbers (990–940 cm^{-1}) than the ν_3 modes (940–750 cm^{-1}) [18–23]. Studies of $Na_2Mo_2O_7$, which contains $Mo_2O_7^{2-}$ units, suggested that the $\nu_{as}MoO_3$ modes give rise to an IR doublet near 825–780 cm^{-1} and the ν_sMoO_3 modes should be observed at higher wavenumbers than the $\nu_{as}MoO_3$ modes [24]. Similarly to phosphates, the $\nu_{as}MoOMo$ modes were observed at higher wavenumbers than the ν_sMoOMo modes [24]. It was also shown that vibrations of the Mo–O–Mo bridge are very sensitive to the Mo–O distances and Mo–O–Mo bond angle, i.e. an increase in the Mo–O interatomic distances is accompanied by a decrease in the wavenumbers of these modes, whereas an increase in the bond angle leads to a shift of the $\nu_{as}MoOMo$ and ν_sMoOMo modes towards higher and lower wavenumbers, respectively [24]. For instance, for the Mo–O–Mo bridge in $Na_2Mo_2O_7$ with the M–O distances 1.90 Å and the Mo–O–Mo angle of 141°, the $\nu_{as}MoOMo$ and ν_sMoOMo modes were observed at 952–942 and 600–525 cm^{-1}, respectively [24]. For $K_3Fe(MoO_4)_2(Mo_2O_7)$ the Mo–O distances are 1.8608(16) and 1.9069(16) Å, and the Mo–O–Mo angle is 162.72(11)°. Since one of the Mo–O distances is shorter and the Mo–O–Mo angle is larger than in $Na_2Mo_2O_7$, one would expect to observe the $\nu_{as}MoOMo$ mode at higher wavenumbers than in $Na_2Mo_2O_7$ and the ν_sMoOMo mode at similar wavenumbers. Our results show that the highest wavenumber modes are observed near 960 cm^{-1}, i.e. at very similar wavenumbers to the $\nu_{as}MoOMo$ mode in $Na_2Mo_2O_7$. Moreover, we do not observe any modes in the 728–423 cm^{-1} range. This result shows that in our case the ν_sMoOMo mode must be observed at significantly higher wavenumbers than the corresponding mode in $Na_2Mo_2O_7$ due

Table 4. Raman and IR wavenumbers for $K_3Fe(MoO_4)_2(Mo_2O_7)$ and the proposed assignment.

Raman						
$z(xx)z$	$x(yy)x$	$x(zz)x$	$z(xy)z$	$x(yz)x$		
A_g	A_g	A_g	B_g	B_g	IR	Assignment
—	—	—	—	—	960vw	Combination
954m	956sh	958sh	951sh	955sh	955vw	ν_1 and $\nu_s MoO_3$
942m	945m	946s	944w	947w	941sh	
928m	930m	929m	930w	932w	930w	
918sh	—	—	—	—	921sh	
—	—	—	—	—	906s	ν_{as}MoOMo
892w	895vw	890w	897w	894vw	891sh	ν_3 and $\nu_{as}MoO_3$
—	—	—	—	—	884sh	
873w	867vw	868w	874vw	868vw	873s	
—	—	—	—	—	870s	
844vw	842vw	843w	—	—	841m	
826w	825vw	828sh	827vw	—	826s	
791m	795w	—	793w	795vw	—	
774w	775m	774w	776vw	776w	771sh	
—	—	—	—	—	758s	
728w	728w	728w	728w	728m	728sh	ν_sMoOMo
—	—	423w	—	—	422m	ν_4
397w	396w	395sh	397vw	392w	383m	ν_4
368sh	369w	371w	368sh	370w	—	ν_4, T' (Fe), δOMoO
350m	—	—	351w	—	357w	ν_2, T' (Fe), δOMoO
—	—	337w	—	339w	339sh	
—	320w	318w	320vw	—	327w	
—	—	—	—	—	304s	
—	281vw	—	—	284vw	276sh	T' (Fe), $T'(MoO_4)$
236w	235w	236m	235vw	234vw	242s	T' (Fe), δMoOMo, $T'(MoO_4)$
226w	220w	—	—	—	—	
193w	197vw	201vw	197vw	203vw	186sh	
—	—	—	—	—	178w	
149vw	—	149sh	—	—	145w	$L(MoO_4)$, T' (K)
—	141w	139w	136vw	142vw	139w	
124vw	—	—	123vw	—	121vw	
—	106vw	102sh	—	—	102vw	
—	—	95m	—	—	95vw	
86w	—	—	87vw	—	86vw	
71m	—	—	71w	—	—	
59m	66vw	62vw	59w	—	58vw	
45m	—	47w	45w	—	49vw	
—	—	36vw	—	—	—	

to some difference in the crystal structure. Indeed, whereas in the $K_3Fe(MoO_4)_2(Mo_2O_7)$ structure the Mo–O–Mo bridges are formed in the isolated $Mo_2O_7^{2-}$ groups (the coordination number of molybdenum is 5), in the $Na_2Mo_2O_7$ structure the Mo–O–Mo bridges are formed between MoO_4 and MoO_6 units sharing vertices to form infinite chains [25]. We assign the Raman band at 728 cm^{-1} to the ν_sMoOMo mode since its energy is too low to justify its assignment to vibrations of the MoO_4^{2-} tetrahedra. As can be noticed, the corresponding band in the IR spectrum is weak and observed only as a shoulder. The former studies of phosphates showed that for a linear P–O–P bridge the ν_s P–O–P mode is observed only in Raman spectra [26, 27]. By analogy with phosphates, we may also expect similar behavior for the ν_sMoOMo mode. The weak intensity of this mode in the IR spectrum can therefore be attributed to the relatively small departure of the Mo–O–Mo angle from linearity. Having in mind that the ν_{as}MoOMo mode should be observed at higher wavenumbers than the $\nu_{as}MoO_3$ and ν_3 modes, and its intensity should be strong in the IR spectrum, we may assign the strong IR band at 906 cm^{-1} to the ν_{as}MoOMo mode. The ν_1 and $\nu_s MoO_3$ modes are observed in the 958–918 cm^{-1} range and the ν_3 and $\nu_{as}MoO_3$ modes give rise to many bands in the 897–758 cm^{-1} range.

Our previous studies in many double molybdates showed that translations of K^+ ions and librations of MoO_4^{2-} ions should be observed below 200 cm^{-1} [18–21]. Translations of the MoO_4^{2-} ions were observed in the 140–300 cm^{-1} region and the internal modes ν_2 and ν_4 of the MoO_4^{2-} ions were found in the 300–510 cm^{-1} range [18–21]. Translations of Al^{3+} and Sc^{3+} ions in $M^I M^{III}(MoO_4)_2$ double molybdates (M^I = Na, K, Rb, Cs; M^{III} = Al, Sc) contributed to modes in the 300–510 and 260–420 cm^{-1} range, respectively [18, 20, 21]. Since the atomic mass of iron is larger than that of scandium and aluminum, translations of the Fe^{3+} ions should be observed at lower wavenumbers than translations of Sc^{3+} and Al^{3+} ions. δOMoO and δMoOMo modes were located in the 300–360 and 180–240 cm^{-1} regions, respectively [24, 28]. We could not find any information on assignment of the rocking modes of the MoO_3 groups and lattice modes of the $Mo_2O_7^{2-}$ ions. We can, however, assume that the lattice modes of these ions should be

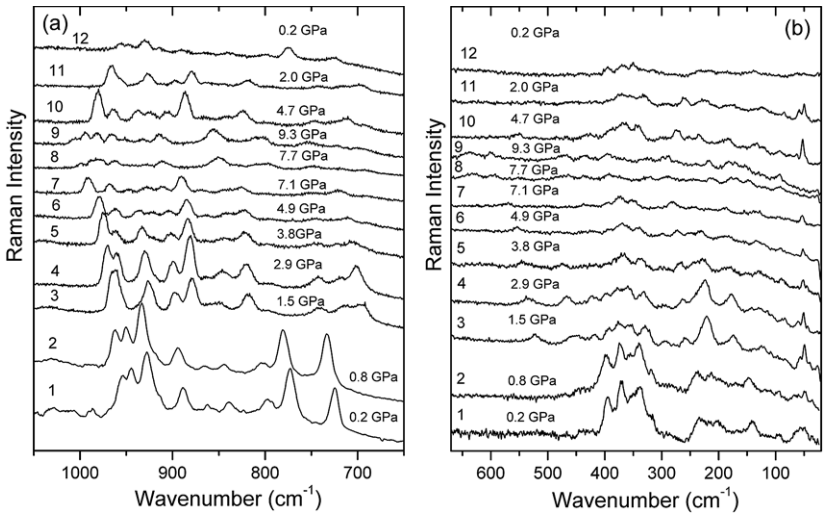

Figure 4. Raman spectra of $K_3Fe(MoO_4)_2(Mo_2O_7)$ recorded at different pressures during compression (spectra 1–9) and decompression (spectra 10–12) experiments. The left (right) panel shows the high (low) wavenumber regions of the spectra. The scattering geometry is close to $x(yy + yz)x$.

observed at lower wavenumbers than the corresponding modes of the MoO_4^{2-} ions due to the significant difference in the mass of these ions. The proposed assignment of the lower wavenumber modes is presented in table 4.

3.3. High-pressure Raman scattering studies

Once a clear picture of the vibrational properties of $K_3Fe(MoO_4)_2(Mo_2O_7)$ is obtained we next discuss the effects of hydrostatic pressure on the structural and vibrational properties of this compound.

The Raman spectra remain qualitatively the same up to 0.8 GPa (see figure 4). At 1.5 GPa pressure significant changes become evident in the Raman spectra, namely (i) new stretching modes appear at 695 and 714 cm^{-1}, (ii) strong changes in intensities of Raman bands are observed and (iii) a new bending mode appears at 523 cm^{-1}. Upon further increase of pressure remarkable changes in the Raman spectra become evident when the pressure is close to 7.4 GPa. Above this pressure the Raman bands experience strong intensity changes, the energy gap between stretching and bending modes almost disappear and the band near 50 cm^{-1} disappears. The observed changes indicate the onset of two pressure-induced phase transitions at about 1.2 and 7.4 GPa.

Further insights into the mechanism of phase transitions in $K_3Fe(MoO_4)_2(Mo_2O_7)$ can be tracked in Raman studies of the $K_3Fe(MoO_4)_2(Mo_2O_7)$ crystal during the decompression. Upon releasing pressure the spectrum of the starting monoclinic phase was recovered, as can be observed in figure 4, thus indicating the reversibility of the processes. However, the intensity of some bands of the starting phase is different before increasing the pressure and after releasing the pressure. This difference is due to some slight reorientation of the sample during the pressure release and creation of defects in the studied sample.

The overall changes in the Raman spectra can be followed in detail by analyzing the wavenumber (ω) versus pressure (P) plot shown in figure 5. For all peaks the $\omega(P)$ behavior can be described using a linear function ($\omega(P) = \omega_0 + \alpha P$). The experimental data were fitted to this expression through the least-squares method. The results for pressure coefficients and wavenumber intercepts at zero pressure are listed in table 5.

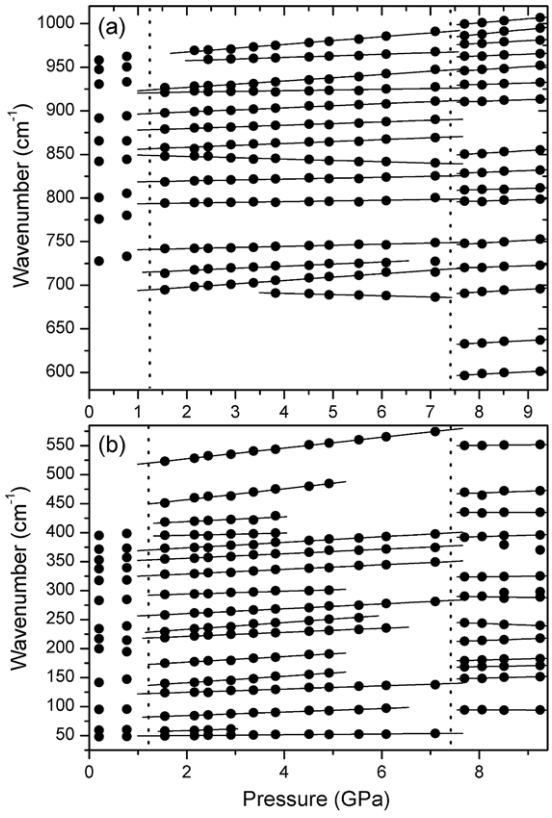

Figure 5. Wavenumber versus pressure plot for the stretching (a) and bending and lattice (b) mode regions during compression. The solid lines are linear fits in the data to $\omega(P) = \omega_0 + \alpha P$. The vertical dotted lines indicate the pressures at which the transitions take place.

Table 5. Pressure intercepts ω_0 and pressure coefficients α for intermediate and high-pressure phases of $K_3Fe(MoO_4)_2(Mo_2O_7)$. For the ambient-pressure phase, the wavenumbers observed at 0.2 GPa are given.

$\omega(P) = \omega_0 + \alpha P$				
Ambient-pressure phase	Intermediate phase		High-pressure phase	
ω (cm^{-1})	ω_0 (cm^{-1})	α (cm^{-1} GPa^{-1})	ω_0 (cm^{-1})	α (cm^{-1} GPa^{-1})
958	958.5	4.40	963.5	4.67
947	953.9	1.82	942.1	5.70
931	919.4	3.71	953.8	2.94
918	919.5	0.86	946.6	2.06
891	893.9	2.38	917.2	3.72
865	875.9	1.89	917.1	1.65
842	853.8	2.19	895.6	1.91
—	850.8	−1.52	824.9	3.27
800	817.5	1.04	811.1	2.27
776	792.5	0.83	798.0	1.46
—	—	—	782.7	1.72
728	739.5	1.28	721.0	3.39
—	712.1	2.43	705.6	1.86
—	690.0	3.86	665.8	3.29
—	696.2	−1.36	—	—
—	—	—	610.7	2.88
—	—	—	573.8	3.02
—	508.8	9.28	541.9	1.06
—	438.0	9.46	443.7	3.09
—	410.9	4.10	434.8	0.02
395	391.7	1.87	—	—
371	364.1	4.80	373.4	2.47
353	348.2	3.88	—	—
337	320.8	3.95	316.8	0.89
317	289.2	2.43	300.1	−1.31
283	252.0	4.17	268.5	−3.13
234	221.1	5.97	—	—
217	214.1	3.48	188.5	3.15
200	166.9	4.85	163.3	2.11
141	129.8	5.66	156.2	1.57
—	119.0	2.79	130.4	2.30
95	78.3	3.07	94.7	−0.07
59	53.3	2.65		
48	48.7	0.68		

The results shown in figure 5 clearly indicate that the material experiences a first structural phase transition at about 1.2 GPa. The analysis of the Raman spectra indicates that this transition has first-order character and the material undergoes significant structural changes. First of all it should be said that this transition leads to significant distortion of the MoO_4^{2-} tetrahedra and $Mo_2O_7^{2-}$ dimers. This is clearly seen, since the stretching and bending modes are spread over broader regions (695–969 and 328–523 cm^{-1}) than in the phase observed below 1.2 GPa, thus meaning a much larger distribution of Mo–O bond lengths. Since the number of modes increases when the phase transition takes place, the high-pressure phase may have lower symmetry than the original one. It is also worth noting that the modes below 100 cm^{-1}, which can be most likely assigned to translations of K^+ ions, are weakly affected by the phase transition. This result suggests that the intermediate phase still has a layered structure. We suppose, therefore, that the application of pressure leads to significant decrease of the *a*-parameter (distance between layers), accompanied by slight rotations of the MoO_4^{2-} and $Mo_2O_7^{2-}$ units. When pressure reaches about 1.2 GPa, a sudden reorganization of the structure takes place through rotations of these units. Upon further increase of pressure, the structure remains stable up to about 7.4 GPa. However, it is worth noting that, in the stability region of the intermediate phase, strong pressure dependence is observed for some stretching modes and near 3.8 GPa a new mode shows up at 691 cm^{-1}. This mode exhibits negative pressure dependence. As a result, the wavenumber region of the stretching modes increases with pressure up to 686–991 cm^{-1} at 7.1 GPa. This behavior clearly indicates that distortion of the MoO_4^{2-} tetrahedra and $Mo_2O_7^{2-}$ dimers increases with pressure, and at about 7.4 GPa a second structural phase transition takes place. Since in the high-pressure phase the gap between the stretching and bending modes almost disappears and no bands are observed below 90 cm^{-1}, the reconstruction of the structure leads most likely to disappearance of its layered characteristics and formation of larger molybdenum–oxygen units with octahedral coordination of the molybdenum atoms.

4. Conclusions

Room-temperature and ambient-pressure x-ray, IR and polarized Raman studies of $K_3Fe(MoO_4)_2(Mo_2O_7)$ have been performed. Moreover, high-pressure Raman scattering studies of this material have been performed at room temperature. The results show that $K_3Fe(MoO_4)_2(Mo_2O_7)$ crystallizes in the layered monoclinic structure. The characteristic feature of this structure is presence of both MoO_4^{2-} and $Mo_2O_7^{2-}$ units. The performed Raman and IR studies allowed us to propose assignment of the observed modes to the respective vibrations of structural units.

The high-pressure results show that the monoclinic phase of this material transforms at approximately 1.2 GPa to another layered phase, which is still built up of the MoO_4^{2-} and $Mo_2O_7^{2-}$ units, but these units are more distorted in comparison with the ambient-pressure phase. Our studies also show that this material exhibits another reversible phase transition when the pressure is close to 7.4 GPa. The coordination of the molybdenum atoms in the high-pressure phase is most likely octahedral. Both transitions are of first order and they are associated with rotations of the MoO_4^{2-} and $Mo_2O_7^{2-}$ units that lead to an increase in electrostatic repulsion between oxygen atoms and consequently lead to the instability of the structures, thus exhibiting a rich phase transformation sequence when pressure varies.

References

[1] Zhang L J, Zhou Y S, Zuo J L, Yu Z, Fun H K, Abdul I and You X Z 2000 *Inorg. Chem. Commun.* **3** 697
[2] Muessig E, Bramnik K G and Ehrenberg H 2003 *Acta Crystallogr.* B **59** 611
[3] Bramnik K G, Muessig E and Ehrenberg H 2003 *J. Solid State Chem.* **176** 192
[4] Soares A P V and Portela M F 2005 *Catal. Rev.* **47** 125
[5] Bowker M, Holroyd R, House M, Bracey R, Bamroongwongdee C, Shannon M and Carley A 2008 *Top. Catal.* **48** 158

[6] Otko A I, Nesterenko N M and Povstyanyi L V 1978 *Phys. Status Solidi* a **46** 577
[7] Mączka M, Pietraszko A, Saraiva G D, Souza Filho A G, Paraguassu W, Lemos V, Perottoni C A, Gallas M R, Freire P T C, Tomaszewski P E, Melo F E A, Mendes Filho J and Hanuza J 2005 *J. Phys.: Condens. Matter* **17** 6285
[8] Klimin S A, Popova M N, Mavrin B N, Van Loosdrecht P H M, Svistov L E, Smirnov A I, Prozorova L A, Krug van Nidda H A, Seidov Z and Loidl A 2003 *Phys. Rev.* B **68** 174408
[9] Jorge G A, Capan C, Ronning F, Jaime M, Kenzelmann M, Gasparovic G, Broholm C, Shapiro A and Demianets Y 2004 *Physica* B **354** 297
[10] Kotova I Y and Kozhevnikova N M 2003 *Russ. J. Appl. Chem.* 2003 **76** 1572
[11] Sebastian L, Sumithra S, Manjanna J, Umarji A M and Gopalakrishnan J 2003 *Mater. Sci. Eng.* B **103** 289
[12] Naruke H and Yamase T 2001 *J. Solid State Chem.* **161** 85
[13] Oxford Diffraction 2002 *CrysAlis RED* version 1.170.14. Oxford Diffraction Ltd, Oxford, UK
[14] Sheldrick G M 1997 *SHELXL97* Program for Solution of the Crystal Structures, University of Goettingen
[15] Cornilsen B C and Condrate R A 1978 *J. Solid State Chem.* **23** 325
[16] Cornilsen B C 1984 *J. Mol. Struct.* **117** 1
[17] Kuhlmann U, Thomsen C, Prokofiev A V, Büllesfeld F, Uhrig E and Assmus W 2001 *Physica* B **301** 276
[18] Maczka M 1996 *Eur. J. Solid State Inorg. Chem.* **33** 783
[19] Maczka M 1999 *J. Raman Spectrosc.* **30** 971
[20] Maczka M, Hanuza J, Lutz E T G and Van der Maas J H 1999 *J. Solid State Chem.* **145** 751
[21] Maczka M, Hermanowicz K, Tomaszewski P E and Hanuza J 2004 *J. Phys.: Condens. Matter* **16** 3319
[22] Paraguassu W, Souza Filho A G, Maczka M, Freire P T C, Melo F E A, Mendes Filho J and Hanuza J 2004 *J. Phys.: Condens. Matter* **16** 5151
[23] Paraguassu W, Maczka M, Souza Filho A G, Freire P T C, Melo F E A, Mendes Filho J and Hanuza J 2007 *Vib. Spectrosc.* **44** 69
[24] Fomichev V V, Poloznikova M E and Kondratov O I 1992 *Russ. Chem. Rev.* **61** 1601
[25] Martin C, Martin I, Rives V and Malet P 1996 *J. Catal.* **161** 87
[26] Baran E J, Botto I L and Nord A G 1986 *J. Mol. Struct.* **143** 151
[27] Mahadevan Pillai V P, Thomas B R, Nayar V U and Lii K H 1999 *Spectrochim. Acta* A **55** 1809
[28] Desikan A N, Huang L and Oyama S T 1991 *J. Phys. Chem.* **95** 10050